Mon. Not. R. Astron. Soc. **000**, 1–17 (2011) Printed 21 March 2014 (MN LATEX style file v2.2)

Chaos in hydrodynamic BL Herculis models.

R. Smolec⋆ and P. Moskalik
N. Copernicus Astronomical Centre, Bartycka 18, 00-716 Warszawa, Poland

arXiv:1403.4937v1 [astro-ph.SR] 19 Mar 2014

Accepted . Received ; in original form

ABSTRACT

We present non-linear, convective, BL Her-type hydrodynamic models that show complex variability characteristic for deterministic chaos. The bifurcation diagram reveals a rich structure, with many phenomena detected for the first time in hydrodynamic models of pulsating stars. The phenomena include not only period doubling cascades en route to chaos (detected in earlier studies) but also periodic windows within chaotic band, type-I and type-III intermittent behaviour, interior crisis bifurcation and others. Such phenomena are known in many textbook chaotic systems, from the simplest discrete logistic map, to more complex systems like Lorenz equations.

We discuss the physical relevance of our models. Although except of period doubling such phenomena were not detected in any BL Her star, chaotic variability was claimed in several higher luminosity siblings of BL Her stars – RV Tau variables, and also in longer-period, luminous irregular pulsators. Our models may help to understand these poorly studied stars. Particularly interesting are periodic windows which are intrinsic property of chaotic systems and are not necessarily caused by resonances between pulsation modes, as sometimes claimed in the literature.

Key words: hydrodynamics – methods: numerical – chaos – stars: oscillations – stars: variables: BL Herculis

1 INTRODUCTION

Chaotic dynamics is present in many astrophysical systems and stellar variability is not an exception, although in this case, chaos was studied mostly in the context of hydrodynamic models of large amplitude pulsators. Buchler & Kovács (1987) and Kovács & Buchler (1988) found a chaotic behaviour in their radiative type-II Cepheid models (W Vir and RV Tau). In depth analysis of chaos in these models was conducted by Serre, Kolláth & Buchler (1996) and Letellier et al. (1996). Also Buchler & Moskalik (1992) found chaotic behaviour in two sequences of radiative BL Her-type models, however did not analyse the phenomenon. Recently chaotic behaviour was reported in convective hydrodynamic models of BL Her stars (Smolec & Moskalik 2012) and RR Lyrae stars (Plachy, Kolláth & Molnár 2013).

On observational side chaos was detected in type II Cepheids of RV Tau type (R Scuti and AC Her; Buchler, Kolláth & Serre 1996; Kolláth et al. 1998) and in several semi-regular variables (Buchler, Kolláth & Cadmus 2004), and in Mira-type variable (Kiss & Szatmáry 2003).

In this paper we report on the chaotic behaviour we have found in a sequence of non-linear convective BL Her models. For the first time in stellar pulsation modelling we clearly demonstrate the appearance of dynamical phenomena well known and common to classical chaotic systems, both discrete (e.g. logistic or Hénon maps) and continuous (e.g. Rössler or Lorenz equations). In all these systems the basic route to chaos is through a cascade of period doubling bifurcations also present in our models and in earlier studies of radiative type-II Cepheid models (Kovács & Buchler 1988). In addition, our models display a full wealth of dynamic behaviour characteristic for deterministic chaos. Within chaotic band we find several windows of non-chaotic variation (windows of order), with stable period-n limit cycles. These windows are either extremely narrow or relatively large. In the latter case the periodic window is preceded by the type-I intermittent behaviour, till the periodic cycle is born through the tangent bifurcation. This periodic cycle again undergoes a series of period doubling bifurcations en route to chaos. The interior crisis bifurcations, in which separate chaotic bands merge, leading to the abrupt increase of the attractors volume are detected in our models, as well as crisis induced intermittency and type-III intermittency.

Chaos was not detected in any BL Her star so far. In our opinion however, these models are important for several reasons. (*i*) Chaos does occur in larger-luminosity type-II Cepheids – RV Tau stars, as well as in semi-regular vari-

⋆ E-mail: smolec@camk.edu.pl

ables. Our models may shed more light on variability of these poorly studied stars. (*ii*) We initiated the survey of non-linear convective pulsation models of type-II Cepheids extending to the highest luminosities (RV Tau domain) in which chaotic variability is expected, as previous radiative models and observations indicate. In the present paper we introduce and test the methods to study chaos in such models. (*iii*) The striking similarity between our hydrodynamic models of pulsating stars and even the simplest chaotic systems, like logistic map, is noteworthy, indicating that many very different systems may share the same dynamical properties. (*iv*) Finally, although the chaotic behaviour was not detected in any BL Her star so far, we cannot exclude such possibility in the future. We note that the period doubling effect in these stars was predicted by Buchler & Moskalik (1992), based on radiative hydrodynamic models, but it took 20 years to discover the effect in the first star of this type (Soszyński et al. 2011; Smolec et al. 2012).

In Section 2 we summarize the properties of the logistic map, which will help us better understand phenomena occurring in our hydrodynamic models. The reader familiar with the chaos theory may safely skip this Section. In Section 3 we briefly describe the computation and basic properties of the models. In the next Sections we present detailed analysis of the models showing both chaotic and periodic variation, including discussion of the largest Lyapunov exponents (Section 5). We discuss our results in Section 6 and comment on observability of the chaotic phenomena in Section 7. Summary in Section 8 close the paper.

Initial results of this study were reported in the conference proceedings of IAU Symposium No 301 (*Precision Asteroseismology*), Smolec & Moskalik (2014).

2 LOGISTIC MAP

In this Section we briefly discuss the properties of the logistic map, which is the simplest 1D discrete system showing deterministic chaos. The map is defined as:

$$x_i = f(x_{i-1}) = kx_{i-1}(1 - x_{i-1}), \qquad (1)$$

where k is a parameter. We are interested in a range $1 < k \leqslant 4$ as then the iterates of eq. (1) are bounded, $x_i \in [0:1]$. For $k < 1$ iterations converge to 0 and for $k > 4$ they diverge. The great advantage of the logistic map is its simplicity – most of the properties, e.g. bifurcation points, fixed points and their stability, may be computed analytically. Full understanding of the mechanisms behind the observed behaviours is thus possible. At the same time logistic map displays nearly all types of behaviours characteristic for deterministic chaos in more complex, continuous and higher dimension systems, that are also present in our hydrodynamic models. In the case of our models analytical approach is not possible and we are left with the complex output of pulsation code. Comparison with results discussed in this Section allows for a better understanding of our hydrodynamical models. The properties of the logistic map described below may be found in numerous textbooks (e.g. Petigen, Jürgens & Saupe 2004) and original articles (e.g. May 1976), and are given here without derivation.

Depending on the value of k the iterations of any initial x_0 (trajectory) either converge to a periodic cycle, or not, and then the chaotic attractor is present. In Fig. 1 we show the bifurcation diagram – a possible long-term values of x_i (initial iterations omitted) as a function of k. The plot is a stack of grey-scaled histograms: for each value of k, we computed several thousand iterations of eq. (1) and calculated the probability with which the iterations fall to one of the 200 bins into which the $[0:1]$ interval was divided. Grey bands of chaos are clearly visible, as well as windows of order in which stable periodic cycles are present. The right part of the figure shows the zoom of the largest, period-3 cycle window.

To visualise the attractor it is useful to construct the first return maps, i.e. plots of x_{i+i} vs. x_i (omitting the initial transient). For the discussion below it is instructive to consider the evolution of return map as k is increased. In a range $2.8 \leqslant k \leqslant 4$ it is shown in the animation that may be found in the online version of this article as additional supporting information.

The consecutive iterates of eq. (1) may be constructed geometrically, using the plot of $f(x)$ vs. x as illustrated in the left panel of Fig. 2 for $k = 2.6$ (thin red line). For initial value x_0 one plots the vertical line towards the f and from that point the horizontal line towards the diagonal, and then repeats the procedure to get a trajectory. In the discussed case it converges to the fixed point, $a_1 = f(a_1)$ (period-1 cycle), which is located at the crossing of f and the diagonal. Its stability depends on the slope of f at the intersection. If the modulus of the slope is less than 1 the iterations converge towards a_1 and the period-1 cycle is stable. It is the case for $1 < k \leqslant 3$: iterations of any x_0 converge towards $a_1 = 1 - 1/k$. For $k > 3$ the slope is steeper than 1, the period-1 cycle becomes unstable and stable period-2 cycle ($a_2 = f^2(a_2)$) is born through the period doubling (pitchfork) bifurcation. The iterates of eq. (1) alternate between two values. The appearance of the period doubling bifurcation is illustrated in the middle panel of Fig. 2 with the help of $f^2(x)$ vs. x plot. For $k < 3$ f^2 intersects the diagonal at a single point corresponding to a stable period-1 cycle. At the bifurcation point ($k_1 = 3$) f^2 is tangent to the diagonal, and for larger k, f^2 intersects the diagonal at three points. The middle point corresponds to the unstable period-1 cycle, which is a degenerate case of period-2 solution. The two other points have the same slopes and correspond to the stable period-2 cycle.

Following the same scenario, at $k_2 = 1+\sqrt{6}$ another period doubling bifurcation occurs giving rise to stable period-4 cycle (and period-2 cycle loses its stability). The cascade of period doubling bifurcations will finally lead to chaos. The extent of the domain of stable period-n cycle ($d_n = k_n - k_{n/2}$) decreases as n increases and the ratio d_n/d_{2n} approaches the Feigenbaum constant ($\delta \approx 4.669$) which is a universal constant for many other systems too (Feigenbaum's universality, see Feigenbaum 1983). Beyond $k_\infty \approx 3.569946$ (the accumulation point) chaos appears for the first time. The described period doubling route to chaos is schematically illustrated in the upper part of Fig. 3 with stable and unstable cycles marked with black solid and red dashed lines, respectively.

Beyond the accumulation point the chaotic domain extends, which however, is densely packed with windows of order – stable period-n cycles. To understand how these are born we focus our attention on the most prominent

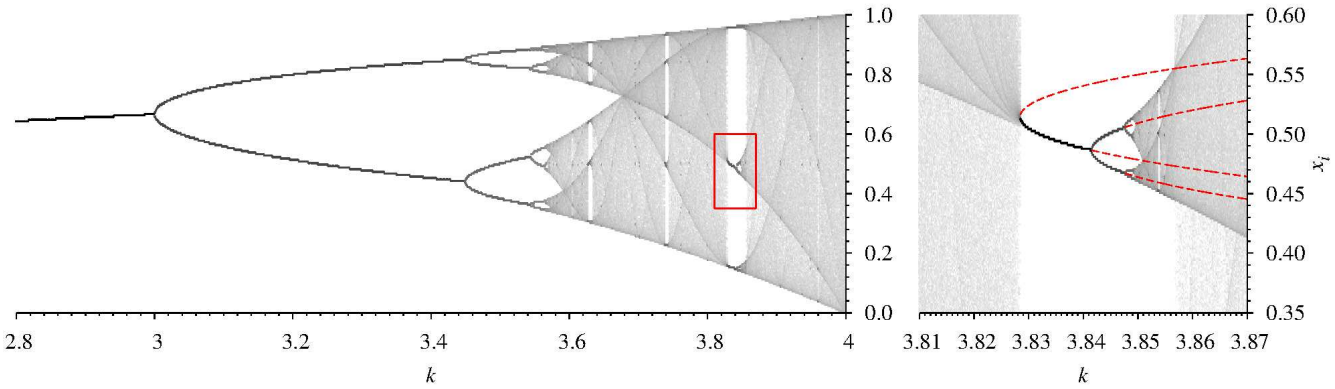

Figure 1. Bifurcation diagram for the logistic map. In the right panel we plot the zoom of the area marked with box in the left panel. Some of the unstable period-3 and period-6 cycles are marked with dashed lines. *[This is low resolution version of the Figure]*

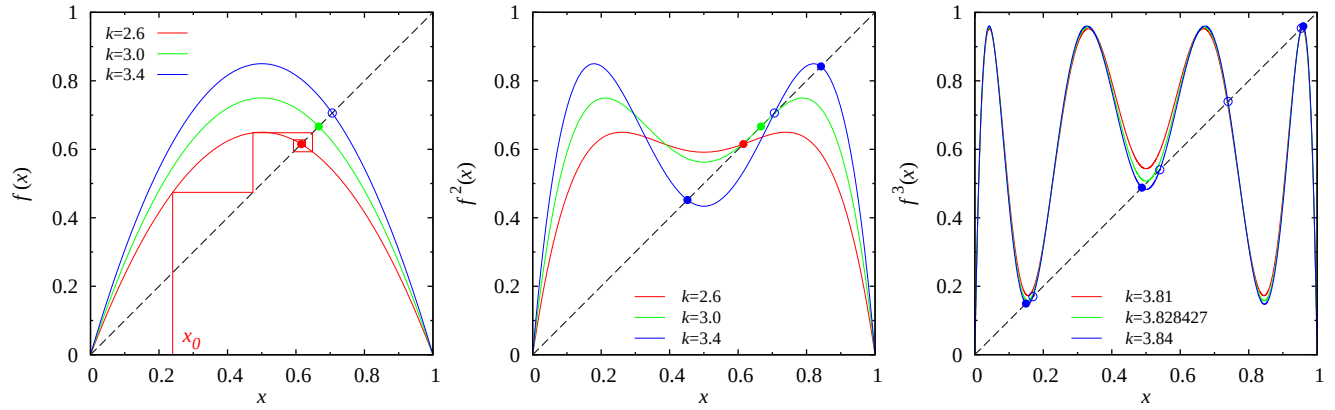

Figure 2. Graphical interpretation of the logistic map. Consecutive iterates of eq. (1) (trajectory) must fall along $f(x)$ curve (parabola). Thin red line in the left panel shows, how to construct the trajectory geometrically for initial x_0. The middle and right panels illustrate the appearance of the period doubling and tangent bifurcations, respectively. In all panels filled and open circles correspond to stable and unstable fixed points, respectively. For clarity, in the right panel these are plotted only for $k = 3.84$.

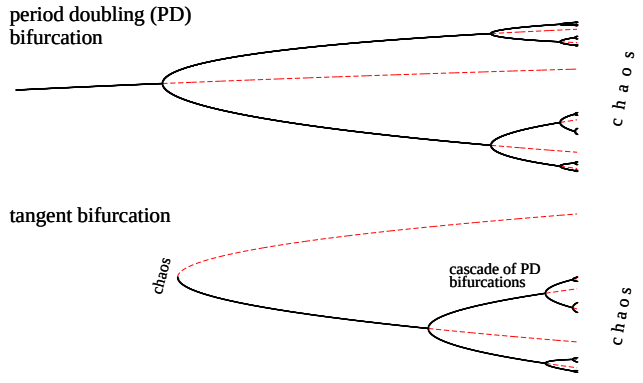

Figure 3. Schematic illustration of the period doubling cascade (top) and tangent bifurcation followed by cascade of period doubling bifurcations (bottom). Black solid and red dashed curves correspond to stable and unstable cycles, respectively.

period-3 window (zoomed in the right part of Fig. 1) and the iteration of f^3 (rightmost panel of Fig. 2). Before the period-3 cycle is born the system is chaotic and the three vertices of f^3 approach the diagonal. At/beyond the bifurcation ($k = 1 + 2\sqrt{2}$) they touch/intersect the diagonal and give rise to a pair of period-3 cycles, of which one is stable and one is unstable, as is apparent from the analysis of the slopes of f^3 at the intersection with the diagonal. The stable period 3-cycle will soon undergo a series o period doubling bifurcations en route to chaos, just as described in the previous paragraphs, and as is clearly visible in the right panel of Fig. 1. This scenario is schematically plotted in the bottom part of Fig. 3.

Two interesting phenomena occur at the edges of the just discussed period-3 window (and other periodic windows as well). Before the tangent bifurcation occurs we observe the intermittency, illustrated in Fig. 4. The bottom panels show the consecutive iterations of eq. (1) for three different values of k and the top panels show the third return maps, i.e. plots of x_{i+3} vs. x_i. Obviously the points fall along the f^3 curve. Just before the bifurcation (left and middle panel) evolution of the system is characterized by long intervals of almost periodic behaviour interrupted by shorter bursts of chaos. This is the intermittent behaviour first analysed for the Lorenz equations by Mannevile & Pomeau (1979), followed by an in-depth analysis by Pomeau & Mannevile (1980). As control parameter increases the almost periodic

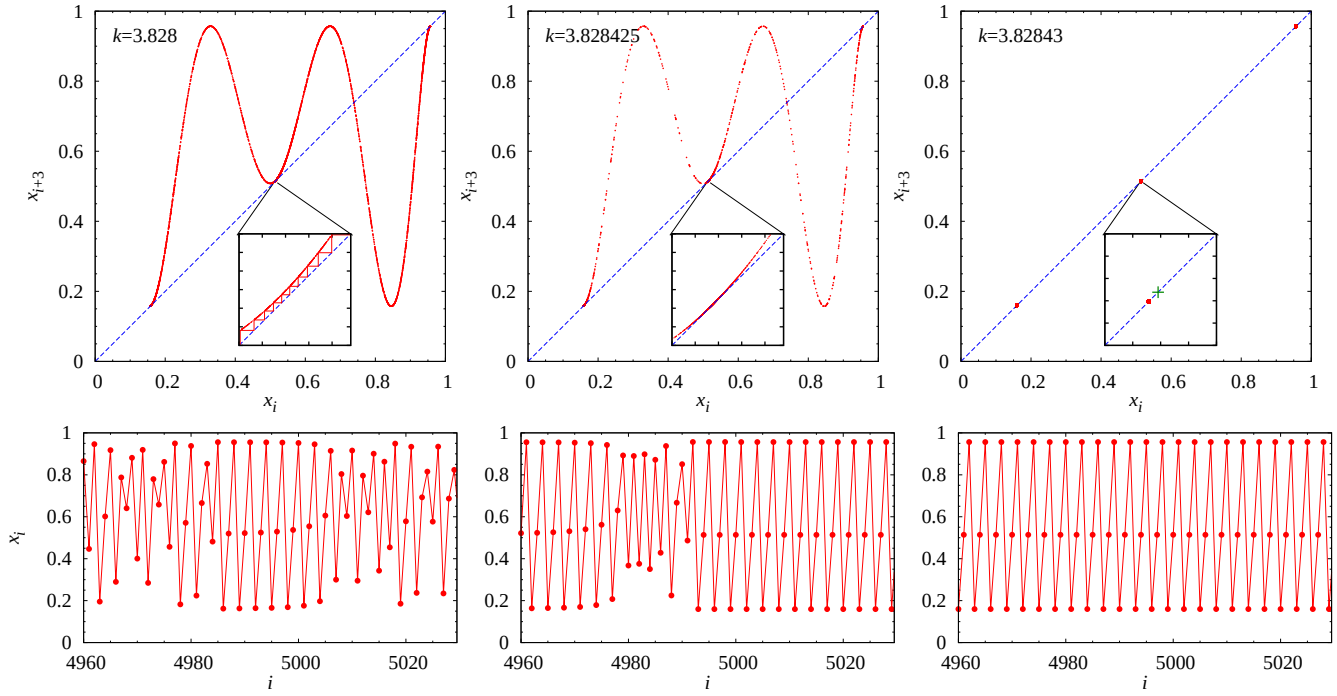

Figure 4. Demonstration of type-I intermittency. The bottom panels show consecutive iterations of the logistic equation for three different values of k. The consecutive iterates are connected with lines for guidance. In the top panels the corresponding third return maps are plotted. In the top right panel (inset) the location of unstable fixed point of period-3 is indicated with +.

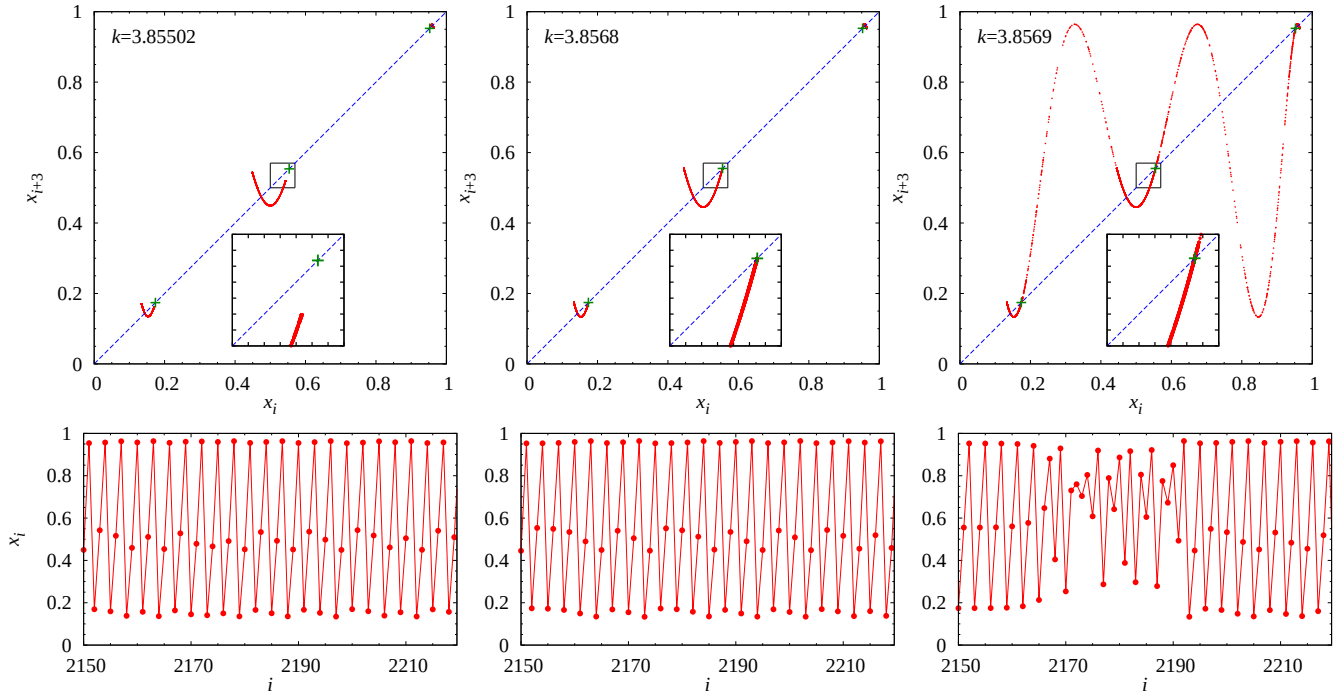

Figure 5. Demonstration of interior crisis. The bottom panels show consecutive iterations of the logistic equation for three different values of k. The consecutive iterates are connected with lines for guidance. In the top panels the corresponding third return maps are plotted. '+' signs mark the location of the unstable fixed points of period-3 born through the tangent bifurcation. See also right panel of Fig. 1, dashed lines.

intervals become longer (cf. left and middle panels in Fig. 4) up to a critical value of k at which tangent bifurcation occurs and stable period-3 cycle is born (and unstable period-3 cycle as well; right panel in Fig. 4).

To discuss the appearance of intermittency we focus attention on the left panel of Fig. 4 (inset). Constructing the trajectory for each third iterate of eq. (1) geometrically, one must fall into the intermittent channel – a narrow region between the vertex of f^3 and the diagonal – in which iterations must be trapped for a while (thin zig-zag in the inset). Similar channels are also present at the two other vertices approaching the diagonal and iterates of eq. (1) fall consecutively into the three channels. Closer to the bifurcation, narrower the channels and longer the iterations are trapped within, with apparently more periodic variation (middle panel of Fig. 4, inset). As the iterations leave the intermittent channels a chaotic burst is observed.

In a broader context, intermittency is one of the routes to chaos (for a review see Eckmann 1981), characterized by sporadic switching between qualitatively different behaviours, the laminar (periodic) behaviour and chaotic bursts. Intermittency is associated with a bifurcation in which stable periodic cycle becomes unstable. Depending on the bifurcation in which the stability is lost, three types of intermittency were distinguished by Pomeau & Mannevile (1980). The type-I intermittency is related to a tangent bifurcation in which stable and unstable limit cycles collide and both vanish. It is the case for the just described intermittency in the logistic map. Type-II intermittency is related to the subcritical Hopf bifurcation (in the Hopf bifurcation the stationary solution bifurcates into periodic orbit)[1]. Type-III intermittency appears together with subcritical period doubling bifurcation, in which the stable limit cycle collides with the unstable period-doubled cycle. A summary of these scenarios may be found in the original paper by Pomeau & Mannevile (1980) and e.g. in Becker et al. (1999). Hydrodynamic models to be discussed in the coming sections display both type-I and type-III intermittency.

The stable period-3 cycle born in the tangent bifurcation will soon undergo a series of period doubling bifurcations which will create three separate chaotic bands as is well visible in Fig. 1 and in Fig. 5 (left and middle panels), which is the same as Fig. 4 except we focus on the right edge of the period-3 window. These three bands will merge in the interior crisis bifurcation, first described by Grebogi, Ott & Yorke (1982), in which the volume of the attractor changes suddenly. The crisis bifurcation occurs as the three chaotic bands hit the unstable period-3 cycle (born in the tangent bifurcation) which scatters the trajectories into previously unvisited regions – Fig. 5 the rightmost panel. This is well visible in the right panel of Fig. 1 in which unstable cycles of period 3 (and period 6) are plotted with the dashed lines and in Fig. 5 where location of unstable fixed points of period-3 is indicated with '+' signs.

Directly after the occurrence of crisis bifurcation, crisis induced intermittency is observed (well visible in the bottom right panel of Fig. 5). The trajectory is confined in the region of the former, pre-crisis attractor, with sporadic excursions out of it.

[1] We follow the convention adopted e.g. in Seydel (2010) and call the bifurcation subcritical if the stable solution exists on one side of the bifurcation point only. If the stable solution exists on either side, the bifurcation is supercritical.

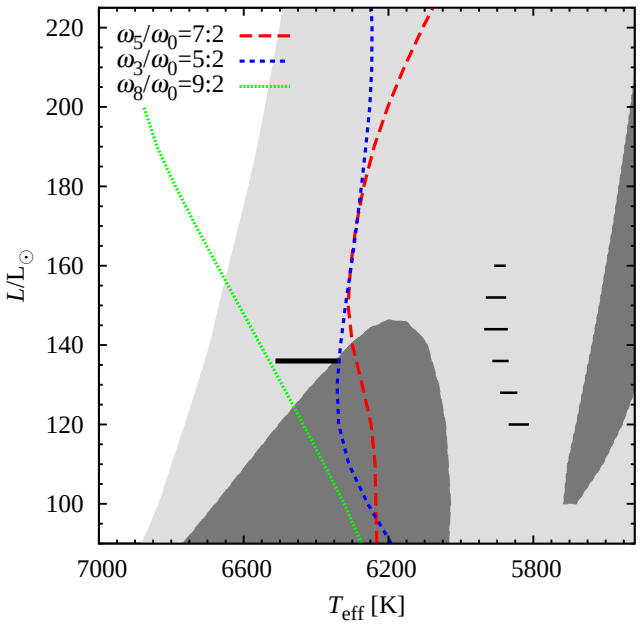

Figure 6. The H-R diagram with the location of models showing chaotic behaviour (thick horizontal line). For reference, models showing periodic and quasi-periodic modulation of pulsation analysed by Smolec & Moskalik (2012) are marked with thin line segments. The light- and dark-shaded areas mark the fundamental and first overtone instability strips, and dashed lines show the loci of some half-integer resonances running close to the analysed models.

3 HYDRODYNAMIC MODELS

All hydrodynamic models analysed in this paper were computed with the Warsaw non-linear convective pulsation codes (Smolec & Moskalik 2008). Numerical parameters of the models (zoning) are the same as in our previous papers (section 3 of Smolec et al. (2012) and Smolec & Moskalik (2012)). The physical parameters of the models and parameters of the turbulent convection model (Kuhfuß 1986) are the same as in Smolec & Moskalik (2012). In particular $M = 0.55\,\mathrm{M}_\odot$, $X = 0.76$ and $Z = 0.0001$. We focus on a single sequence of models with the same luminosity, $L = 136\,\mathrm{L}_\odot$ and varying effective temperature, $T_{\rm eff}$, which is our *control* parameter through this paper. The models cover a strip extending over 170 K, from 6340 K to 6512 K (corresponding periods of the fundamental mode are 1.696 d and 1.527 d). The maximum temperature difference between the consecutive models is only 1 K and in the most interesting domains the difference is as small as 0.1 K. In Fig. 6 we show the location of our models in the H-R diagram (thick horizontal line), together with the location of models that we have studied in Smolec & Moskalik (2012) that show periodic and quasi-periodic modulation of pulsation (thin horizontal lines).

In non-linear computations, the initial static model was perturbed with the velocity profile, and was integrated for at

least 10 000 pulsation cycles with 1 200 time steps per pulsation cycle. By default, all the models were initialized in the same manner, with velocity eigenfunction of the fundamental mode, scaled to match the $4.5\,\mathrm{km\,s^{-1}}$ surface velocity. To check for the possible dependence of results on the initialization, in particular to check whether e.g. two attractors are possible for the same model (hysteresis), several models were initialized in a different manner (with larger surface velocity or with a mixture of the fundamental mode and first overtone eigenfunctions). In all considered cases, the computations converged to the same attractor, only the length of the initial transient phase was different. To check the long-term stability of the computed attractors (either periodic or chaotic), we have computed up to 50 000 pulsation cycles for a few models. In all cases the attractor emerging from the calculation of first 10 000 pulsation cycles remained stable.

We note that in these models the eddy-viscous dissipation is strongly decreased, $\alpha_m = 0.05$ (for equations see Smolec & Moskalik 2008). It results in significant pulsation amplitudes and, as our treatment of radiation is very simple (diffusion approximation) and model mesh is fixed, in erratic light curves with spurious spikes (see section 4 in Smolec & Moskalik (2012) for detailed discussion of this point). Therefore in this paper we analyse the radius variation only, which is smooth. In Fig. 7 we plot a section of typical time series for model showing chaotic variability (6410.0 K).

4 ANALYSIS OF THE BL HER HYDRODYNAMIC MODELS

In this Section we analyse the radius variation of our hydrodynamic models.

4.1 Bifurcation diagram

Deterministic chaos is present in our models beyond doubt. The conclusion is unavoidable once the bifurcation diagram is plotted – Fig. 8. The diagram is constructed in a similar way as in the case of logistic map (Fig. 1). For each value of our control parameter – the effective temperature – we computed the probability that the maximum radii, $R_{\max}$, falls into one of the 120 bins into which the range of radius variation in our models ($\sim 11.0 - 12.7\,\mathrm{R}_\odot$) was divided. The stack of grey-scaled histograms is displayed in Fig. 8 and shows a striking similarity to classical chaotic systems. One can pick other parameter than maximum radius to construct the bifurcation diagram, but results are qualitatively the same. As compared to Fig. 1 the bifurcation diagram looks rough which results from smaller resolution in the control parameter and decreased number of bins along vertical axis, necessary to have a reasonable statistics in each bin.

On both sides of the computation domain single-periodic (cycle-1) pulsation in a fundamental mode is present. The chaotic bands are reached through a series of period doubling bifurcations both from the cool and the hot side. Qualitatively the same scenario is observed for the Gauss (or *mouse map*), see e.g. Hilborn (2000). The chaotic bands are separated with periodic windows of order. The largest period-3 window is nearly a one-to-one copy of the just discussed counterpart seen in case of the logistic map. Within chaotic bands pronounced structures are clearly visible as well – the probability of hitting particular bins by maximum radii is not equal. Some values of maximum radii are clearly preferred as indicated with darker bands, migrating across the bifurcation diagram as control parameter changes.

4.2 Period doubling cascade en route to chaos

Our hydrodynamic models display two pronounced period doubling cascades that lead from a single-periodic fundamental mode pulsation (period-1 cycle) to chaos. The first cascade extends on the cool side of the computation domain. We clearly observe the appearance of period-2 cycle (first in the 6344.0 K model and present up to 6350.0 K model) and period-4 cycle (first in the 6351.0 K model and present also in the 6352.0 K model). Further periodic cycles are not resolved in our model grid with 1 K step in effective temperature. The maximum radii of the 6353.0 K model are bounded within eight well separated chaotic bands, which, as effective temperature is increased, merge smoothly into one chaotic band (at 6355.0 K).

The other period doubling cascade, on the hot side of the computation domain, extends over much larger temperature range, but otherwise it is a mirror image of the just discussed cascade. The consecutive period doubling bifurcations occur with decreasing control parameter. For such situation, the terms period-halving or inverse period doubling cascade are in use. Here we describe the route from order (period-1 cycle) to chaos as effective temperature is decreased. Period-2, period-4, period-8 and period-16 cycles are all clearly detected. They appear for the first time in models with temperatures 6508.0 K, 6490.0 K, 6485.0 K and 6484.0 K, respectively. Period-8 and period-16 variation is detected in only one model each. In 6483.0 K model maximum radii are bounded within four separate chaotic bands.

It is interesting to check whether the lengths of the domains of the consecutive period-n cycles follow the Feigenbaum scaling. Our model grid is too coarse to exactly pinpoint the bifurcation points and hence only a rough estimates are possible. Assuming that the bifurcation occurs halfway between the neighbouring period-n and period-$2n$ models we get (for the cascade on the hot side): $d_2 = 18\,\mathrm{K}$, $d_4 = 5\,\mathrm{K}$ and $d_8 = 1\,\mathrm{K}$ for the extents of the period-2, period-4 and period-8 domains, respectively (see Section 2). The ratios (assuming 0.5 K error in the estimate of the bifurcation point) are $d_2/d_4 = (3.6 \pm 0.4)\,\mathrm{K}$ and $d_4/d_8 = (5 \pm 2.5)\,\mathrm{K}$ not significantly different from the Feigenbaum constant ($\delta \approx 4.669$) toward which the ratio d_n/d_{2n} converges as $n \to \infty$ for the logistic map and other iterated maps, too (Feigenbaum 1983; Collet, Eckmann & Lanford 1980; Collet, Eckmann & Koch 1981). Feigenbaum scaling is also observed with periodic solutions of the ordinary differential equations (Seydel 2010). For the cascade on the cool side we may only estimate d_2/d_4 which is $(3.5 \pm 0.9)\,\mathrm{K}$.

4.3 Case studies 1: chaotic models

Before we describe the phenomena that shape the bifurcation diagram, we present a more detailed analysis for three chaotic models (6410.0 K, 6450.0 K and 6476.0). Their location in the bifurcation diagram (Fig. 8) is shown with black

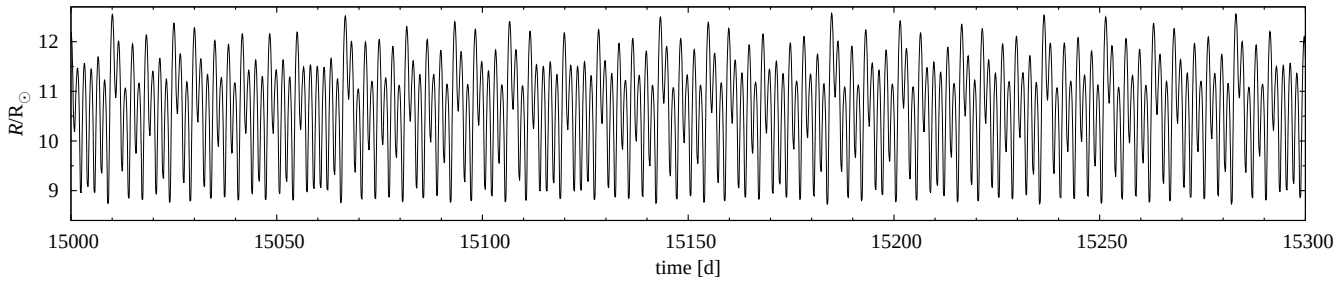

Figure 7. Section of time series for 6410.0 K model showing chaotic variability.

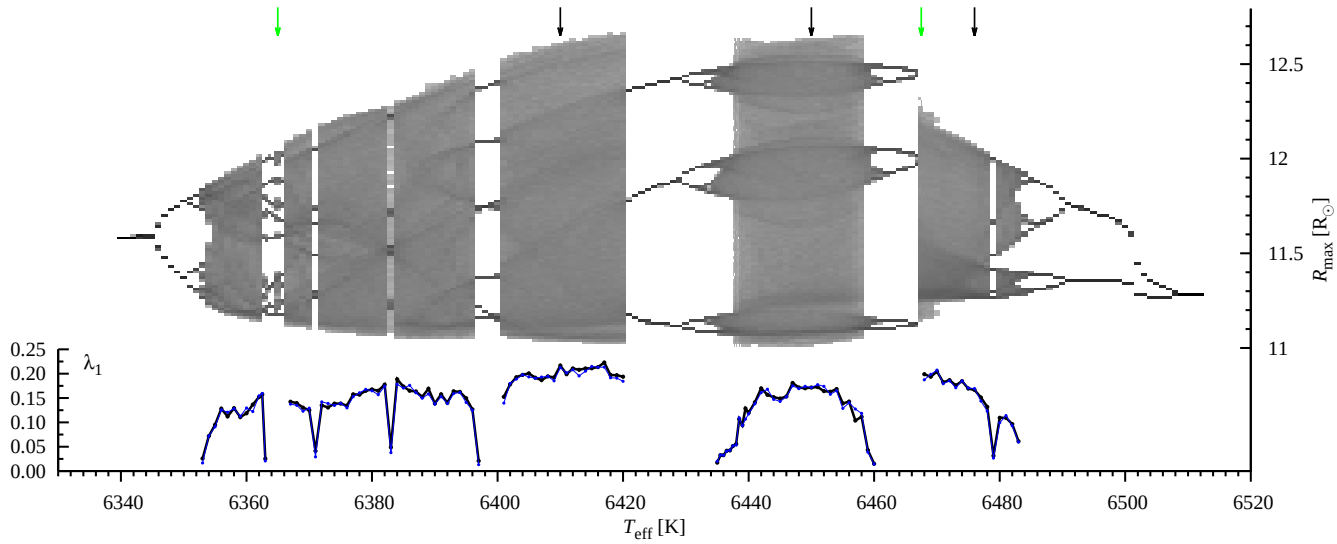

Figure 8. Bifurcation diagram for hydrodynamic BL Her models constructed with values of maximum radii over 9 000 pulsation cycles. Arrows in the top section point the location of particular chaotic (black arrows) and periodic (green arrows) models discussed in Sections 4.3 and 4.6, respectively. In the bottom we plot the largest Lyapunov exponents for the chaotic models – see Section 5 for details.

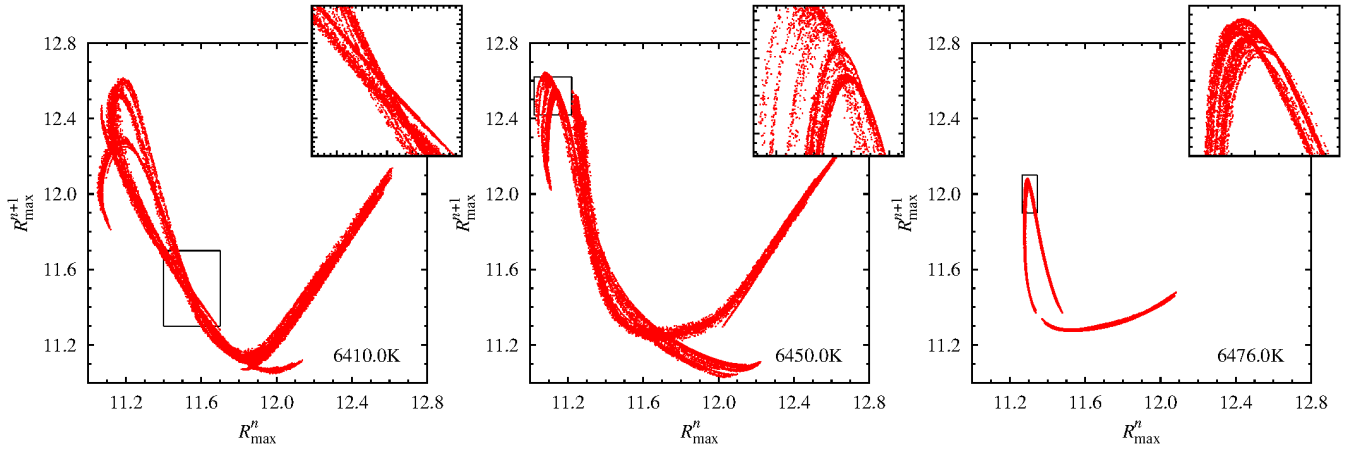

Figure 9. First return maps for three chaotic models (marked with arrows in Fig. 8). Data for the last 46 000 cycles (out of 50 000 computed) are plotted. *[This is low resolution version of the Figure]*

arrows. Nearly all of the computed chaotic models were analysed in the same manner as presented below.

There is not much to learn from the time-series alone. As an example in Fig. 7 we show radius variation over ≈ 180 pulsation cycles for 6410.0 K model, and indeed, no obvious regularity can be noticed. Much more useful are return maps for maximum radii, ie. plots of $R^{n+1}_{\rm max}$ vs. $R^{n}_{\rm max}$. These are Poincaré maps with surface of section defined by $dR/dt = 0$ at maximum expansion phase. The maps are shown in Fig. 9 for the discussed models. The points do not populate the plot in a random manner but fall along a characteristic, albeit rather complex shape, which evolves as the effective temperature changes. This evolution is illustrated with animation that may be found in the online version of this article as additional supporting information (see also other maps for chaotic models of different effective temperatures – grey dots in Figs. 11 and 13). The complex shape, as compared to analogous maps for some classical systems (e.g. tent map for the maximum z values in the Lorenz system, see Lorenz (1963) or in Petigen, Jürgens & Saupe (2004)) is not surprising. Our system is much more complex and return map is only a 2D projection of complex dynamics occurring on a higher dimension manifold. The insets in Fig. 9 provide insight into the fine-structure of the chaotic attractor. Although the numerical noise does not allow to show the cascade of such zoom-ins into smaller and smaller regions we conclude that the attractor's structure is most likely fractal and the attractor is strange.

Chaos clearly manifests in the Fourier spectra, which are plotted in Fig. 10. In each case a time series for $\approx$ 650 pulsation cycles was analysed with Period04 software (Lenz & Breger 2005). The spectra were pre-whitened with the frequency of the fundamental mode and its harmonics – location of these frequencies is shown with dashed lines. For two models also additional highest-signal frequencies in the resulting spectra were pre-whitened and the result is also shown in Fig. 10.

In each case wide bands of signal are present in the spectra, which are characteristic signature of chaos. One large band is present for the 6410.0 K model (Fig. 10, top panel), without any obvious structure. To the contrary, in the case of the 6450.0 K model (Fig. 10, middle panel), wide bands are concentrated around $1/3 f_0$ and its harmonics. The cause of this difference becomes clear once the bifurcation diagram is analysed (Fig. 8). In the case of 6410.0 K model there are no obvious preferred values, or ranges of values, for the maximum radii. For the 6450.0 K model, the maximum radii fall preferentially into three ranges which manifest in Fig. 8 as three dark-grey bands within one large chaotic domain extending between 6438.0 K and 6458.0 K. The signal at $1/3 f_0$ and its harmonics is obviously not coherent which successive pre-whitening (see Fig. 10) shows.

The situation is slightly different for the 6476.0 K model (Fig. 10, bottom panel). After pre-whitening with the fundamental mode and its harmonics strong signal is present at subharmonic frequencies. It results from the two-band structure of the attractor clearly visible in the return map (Fig. 9, right panel). The maximum radii alternate between the two bands and vary chaotically within each of them. Therefore, signal at $1/2 f_0$ and its harmonics is strong and highly coherent but, after pre-whitening with these frequencies, only very wide bands of signal without any obvious structure are present in the frequency spectra.

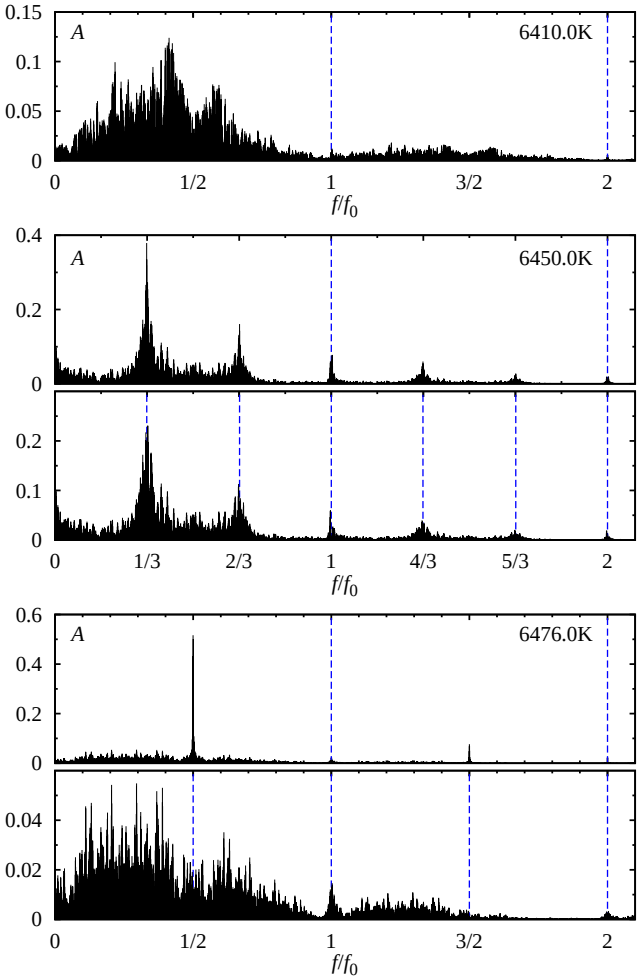

Figure 10. Fourier spectra for three models of different effective temperature showing chaotic behaviour. Dashed lines show the location of pre-whitened frequencies (fundamental mode and harmonics in each case, and additional frequencies for the 6450.0 K and 6476.0 K models.

4.4 Periodic windows of order

Within the chaotic band (Fig. 8) seven windows, in which much more ordered behaviour is observed, including strictly periodic variation, may be identified. Below they are briefly described in the order they appear as effective temperature is increased. The return maps for some of the models are plotted in Figs. 11, 12 and 13. In each case the neighbouring chaotic model (of lower effective temperature) is plotted with grey points for reference. The most interesting period-3 window is discussed in more detail in Section 4.5 and two interesting models from period-6 and period-9 windows are discussed in Section 4.6

Period-9 window is present for models in a range 6363.0 − 6366.0 K (Fig. 11). In fact this window is not strictly periodic but display a complicated internal structure. Within this window models were computed with a smaller 0.5 K-step in effective temperature. For all models

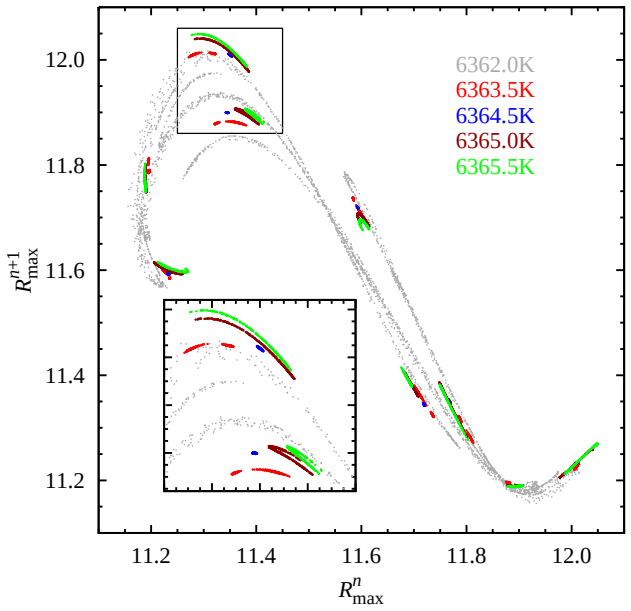

Figure 11. First return map for four models located within period-9 window. For a reference, the return map for the closest and cooler chaotic model is plotted with grey dots. Data for the last 3 000 pulsation cycles out of the total 10 000 computed cycles are plotted.

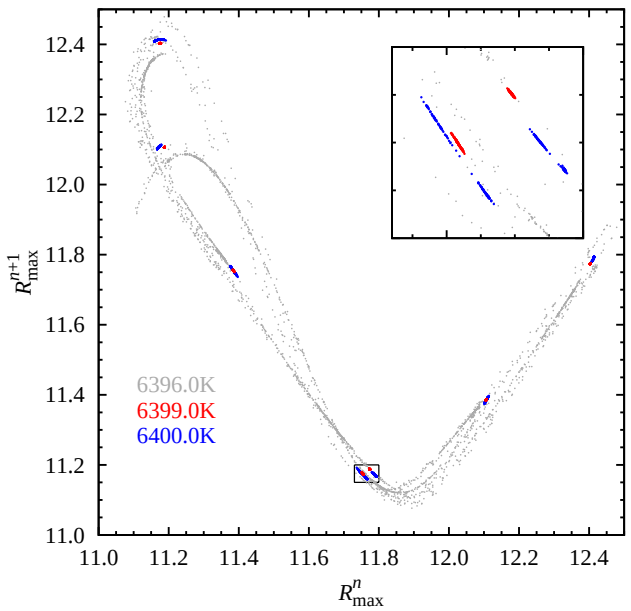

Figure 12. First return map for two models located within period-7 window. For a reference, the return map for the closest and cooler chaotic model is plotted with grey dots. Data for the last 3 000 pulsation cycles out of the total 10 000 computed cycles are plotted.

nine bands are clearly visible, which are either very wide (6365.0 K, 6365.5 K) or very narrow (6364.5 K) indicating a possible strict period-9 cycle. In the case of 6363.5 K model each of the nine bands is split and thus 18 bands are apparent. A detailed analysis of the 6365.0 K model (that shows a rare case of type-III intermittency) is presented in Section 4.6.

Period-6 window is present for one model of 6371.0 K (Fig. 13a). The neighbouring ±1 K models display one chaotic band. Certainly our model grid lacks resolution to provide more insight into the dynamic scenarios within such a narrow window. In return map six very small bands rather than points are present, and thus model is not strictly periodic. The periodic model might be located just a tiny fraction of Kelvin away. This remark also applies to other very narrow windows discussed below.

Period-5 window is present for one model of 6383.0 K (Fig. 13b). The neighbouring ±1 K models display one chaotic band. Detailed analysis shows that in fact for this model the maximum radii form five narrow chaotic bands which may join during the *chaotic bursts* for several pulsation cycles. Two such bursts happened within 10 000 cycle integration of the model and are illustrated in Fig. 14. In this model we also detect a signature of type-III intermittency: switching between period-5 cycle and period-10 cycle. Since the effect is barely visible for this model, we postpone its discussion to Section 4.6, in which we present a more clear example of type-III intermittency in one model in period-9 window.

Period-7 window is present for models in a range 6397.0 − 6400.0 K (Fig. 12). In-between 6399.0 K and 6400.0 K period doubling bifurcation occurred. As inset in Fig. 12 shows, each of the seven, very narrow bands present in the 6399.0 K model is split into two wider bands in the slightly hotter, 6400.0 K model.

Period-3 window with subsequent period doubling cascade extends between 6421.0 K (period-3 cycle) and 6438.0 K (three chaotic bands). This largest window is discussed in detail in the next Section.

Period-6 window with subsequent (inverse) period doubling cascade. The window extends between 6459.0 K, at which three chaotic bands are present, till 6468.0 K at which period-6 cycle, reached through the inverse period doubling cascade, ceases to exist. This window is in fact a mirror image of the just discussed period-3 window, except the (inverse) period doubling cascade seems to be truncated at the cease of period-6 cycle, which is followed by chaos instead of stable period-3 cycle. The scenario around 6468.0 K is uncommon and will be discussed in more detail in Section 4.6 and in Section 6.

The latter two windows represent a clear example of **period-3 bubble** (or *remerging Feigenbaum tree*, Bier & Bountis 1984). The outlook at the bifurcation diagram (Fig. 8) reveals that the two just discussed windows are in fact tightly connected. The scenarios at the cool and hot side of the chaotic band separating the windows and extending between 6438.0 − 6459.0 K are not only mutual mirror images. In fact the three chaotic bands formed at the two sides of the chaotic domain do not disappear as they merge into one chaotic band (in the interior crisis bifurcation, see next Section), but sustain their identity and smoothly merge within the chaotic domain as the dark-grey bands in Fig. 8 indicate.

Period-6 window is present for one model of 6479.0 K (Fig. 13c). The neighbouring ±1 K models display two chaotic bands. The ones at the cool side merge into one band at 6475.0 K.

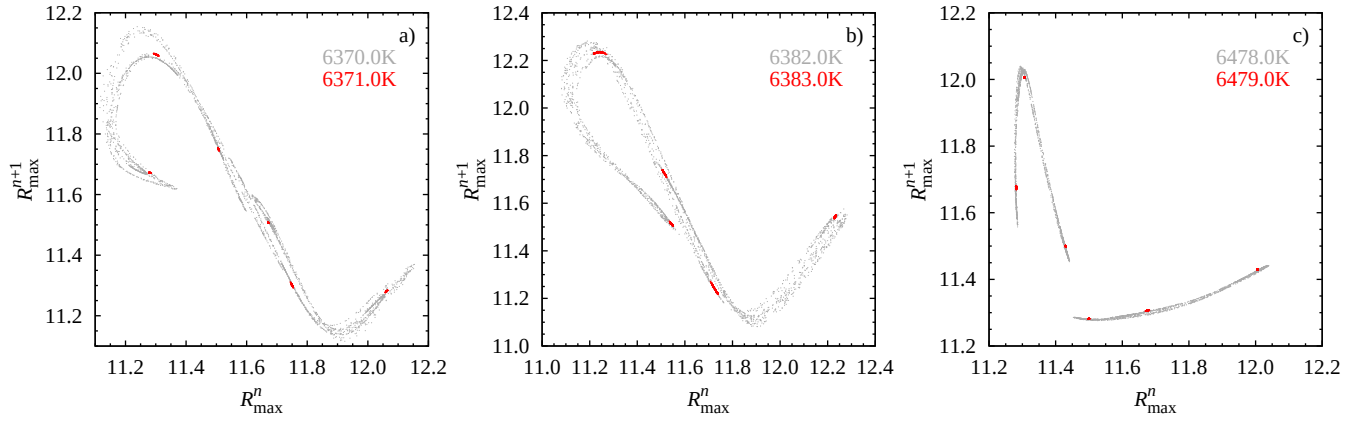

Figure 13. First return maps for models within different periodic windows: a) period-6 window, b) period-5 window and c) period-6 window discussed in Section 4.4. In each case the the return map for the closest cooler chaotic model is plotted with light-grey dots for reference. In each case data for the last 3 000 pulsation cycles out of the total 10 000 computed cycles are plotted.

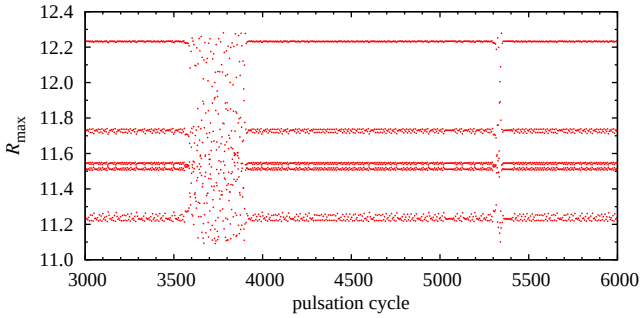

Figure 14. Values of maximum radii plotted over 3 000 pulsation cycles for 6383.0 K model showing a complex variation with chaotic bursts (at pulsation cycles between $3\,600 - 3\,900$ and at 5 800).

4.5 Intermittency and crisis at period-3 window

In this Section we focus attention on the largest period-3 window extending between 6421.0 K and 6438.0 K, and its direct vicinity. For the most interesting temperature ranges, at the edges of the window, the models were computed with a very small, 0.1 K-step in effective temperature. The corresponding part of the bifurcation diagram displays a striking similarity to the bifurcation diagram of the logistic map, Fig. 1, and bifurcation diagrams of many other dynamical systems (e.g. Rössler system, see in Petigen, Jürgens & Saupe 2004). This similarity, and the analysis presented in this Section, lead to conclusion that in these systems the same dynamical phenomena lead to the appearance of the period-3 window and its subsequent evolution to chaos.

In Fig. 15 (top two panels) we show the values of maximum radii during the 1 500 pulsation cycles in two models directly preceding the appearance of the period-3 window. Intermittency is clearly visible. For the 6420.7 K model the intervals with apparently periodic, period-3 variation are short, last by up to 50 pulsation cycles, and are interrupted by much longer intervals of chaos. As the period-3 window is approached the almost periodic behaviour dominates, as is the case for the slightly hotter model of 6420.9 K. The long intervals of period-3 behaviour are only sporadically interrupted with much shorter bursts of chaos. This behaviour is characteristic for type-I intermittency. The appearance of intermittency and the birth of the period-3 window are further illustrated in Fig. 16. It shows the third return maps (top) and small sections of radius variation for three different models at the onset of period-3 window. The Figure is a counterpart of Fig. 4 for the logistic map. The intermittent behaviour is well visible in the models directly preceding the period-3 window. The return maps show the formation of the intermittent channels (one is zoomed in the insets for 6417.0 K and 6420.9 K models), which get narrower as effective temperature is increased and bifurcation point is approached. As system evolves through the intermittent channels the apparently periodic variation is observed. For the hotter model, the density of points at the very narrow intermittent channel is high indicating long intervals of periodic variation. This is also illustrated with the sections of radius variation (bottom panels of Fig. 16) which were chosen to show the almost periodic variation interrupted with short chaotic burst (at $\approx 19\,296$ d for 6420.9 K model). In between 6420.9 K and 6421.0 K the intermittent channel touches the diagonal and period-3 cycle is born in the tangent bifurcation (rightmost panel in Fig. 16).

The ensuing scenario follows the one depicted schematically in the lower part of Fig. 3 and discussed in more detail for the logistic map (Section 2). As effective temperature is increased, the period-3 cycle undergoes a series of period doubling bifurcations en route to chaos. The first bifurcation takes place at ≈ 6429.0 K and leads to period-6 cycle. The model at 6434.0 K is a period-12 cycle. Further period doublings are not resolved in our computations and the following models display a 6-band chaos and finally 3-band chaos.

The three chaotic bands merge in an interior crisis bifurcation which is illustrated with the help of Fig. 17, which should be analysed together with its counterpart for the logistic map – Fig. 5. For the first two models 3-banded chaos is present – the values of maximum radii are bounded in three, well separated ranges, which is clearly visible both in the return maps and in the sections of radius variation. At the tangent bifurcation leading to the appearance of period-3 window the unstable period-3 cycle was also created. Its

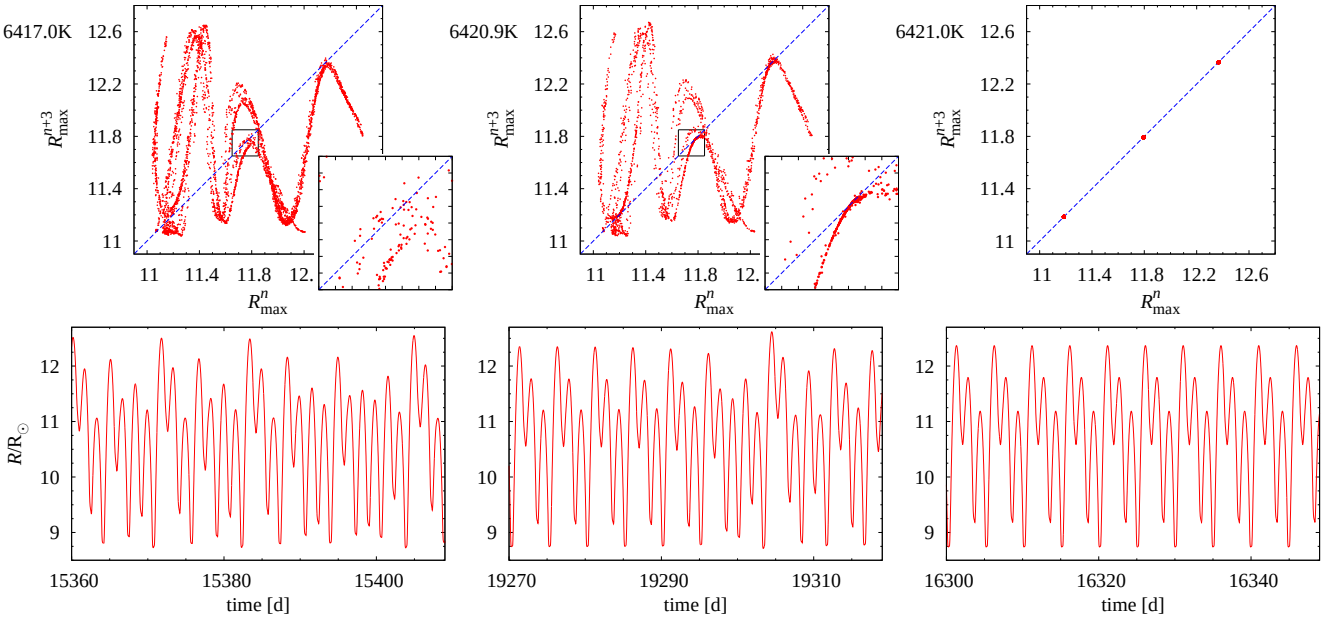

Figure 16. Illustration of type-I intermittency at the onset of period-3 window. The top panels show the third return maps and the bottom panels show the sections of radius variation for three models of different effective temperature. Note that the last two models are separated by 0.1 K, only. Compare with Fig. 4 for the logistic map.

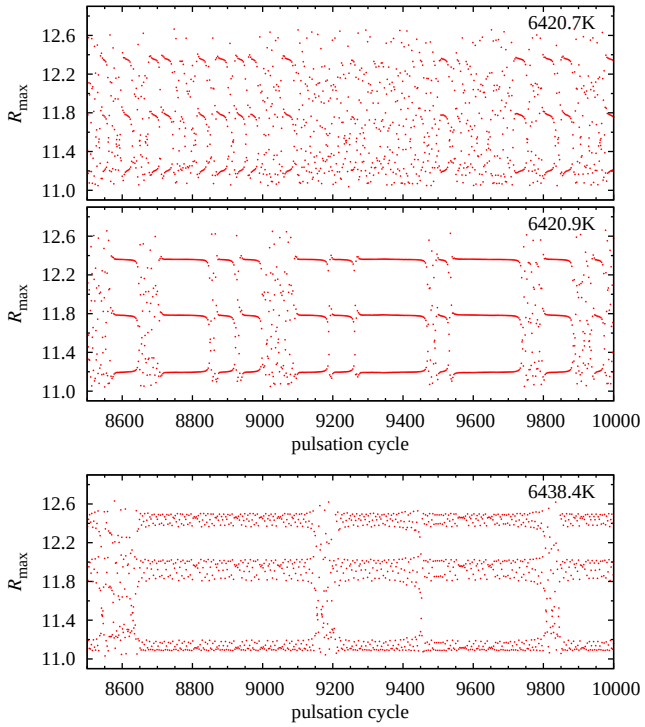

Figure 15. Maximum radii plotted over 1 500 consecutive pulsation cycles for three models showing the type-I intermittency (top two panels) and crisis induced intermittency (bottom panel).

exact location in the return map cannot be computed as was the case for logistic map, but the corresponding three points must be located at the diagonal. As effective temperature is increased (cf. left and middle panels of Fig. 17) the three chaotic bands expand, approaching the diagonal and the anticipated unstable period-3 cycle, location of which may now be easily guessed. At the interior crisis bifurcation the three-band chaotic attractor collides with the unstable period-3 cycle and expands into one-band chaotic attractor.

Directly after the crisis bifurcation, the maximum radii still fall preferentially into the ranges defined by the three chaotic bands. It is well visible in the return map in the rightmost panel of Fig. 17 (higher density of points along the three extended arches) and in the corresponding section of radius variation. In addition in Fig. 15 (bottom panel) we plot the values of maximum radii during the 1 500 consecutive pulsation cycles for the same model. For many pulsation cycles the system evolves in a phase-space defined by the former three-band chaotic attractor and only sporadically gets scattered over a larger space. This behaviour is called *crisis induced intermittency* and ceases as effective temperature is increased, albeit, still the probability of maximum radii falling into one of the three bands is larger thorough the full chaotic domain separating the period-3 and period-6 windows (6438.0 − 6458.0 K; see Fig. 8).

4.6 Case studies 2: periodic models

In this Section we discuss in more detail two models displaying periodic variation: 6467.5 K and 6365.0 K models. In the bifurcation diagram (Fig. 8) their location is indicated with green arrows. The first model is located within period-6 window while the second is located within period-9 window. Figs. 18 and 19 show the frequency spectra for the two models. For clarity, these are limited to $[0, f_0]$ range.

As arrow in Fig. 8 indicates 6467.5 K model is located at the border of chaotic band and period-6 window. Whether it is in fact a period-3 cycle variation, just a moment before the period doubling bifurcation, or period-6 cycle, just after the bifurcation, is not clear from the bi-

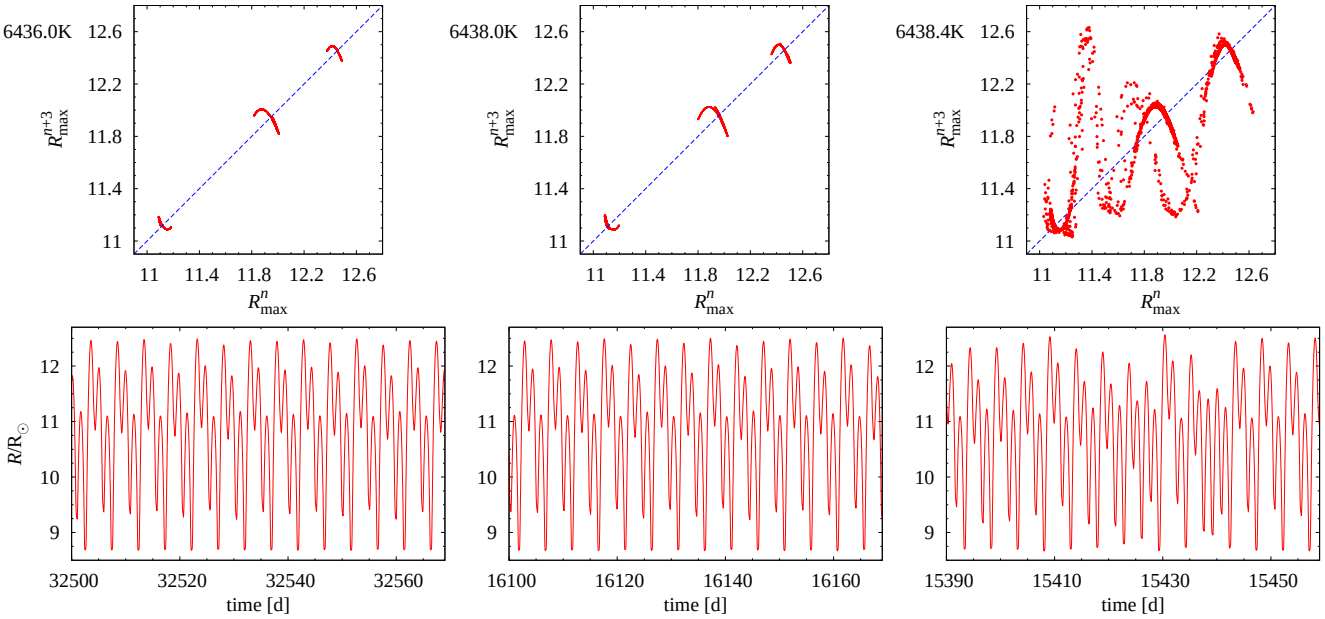

Figure 17. Illustration of interior crisis at the cease of period-3 window. The top panels show the third return maps and the bottom panels show the sections of radius variation for three models of different effective temperature. Compare with Fig. 5 for the logistic map.

furcation diagram. Analysis of return map, which consists of three slightly elongated clumps extending over less than $0.01\,R_\odot$ does not provide the clue, either. Before we discuss the Fourier spectrum for the considered model, we briefly describe other method that may be used to resolve the issue, which we find particularly useful for similar models at the direct vicinity of bifurcation points. We analyse growth of the maximum kinetic energy of the model, from one pulsation cycle ($E^i_{\rm kin,max}$) to other ($E^{i+1}_{\rm kin,max}$). The corresponding kinetic energy growth rate, which we define as $\gamma = 2(E^{i+1}_{\rm kin,max} - E^i_{\rm kin,max})/(E^{i+1}_{\rm kin,max} + E^i_{\rm kin,max})$, summed over k pulsation cycles, γ_k, should be close to zero for the period-k limit cycle. The method has thus additional advantage of pointing whether variations converge to limit cycle, or not. In the bottom panel of Fig. 20 we plot both γ_3 and γ_6 for the considered model. For a reference, in the top panel we plot γ_1 for a singly-periodic 6332.0 K model located well beyond the chaotic domain. The mean value of γ_1 for this model is zero, as expected. The small ($\sigma = 3 \cdot 10^{-5}$) fluctuations around the mean result partly from the interpolation (the time step is not an integer part of the period) and partly from the numerical noise which is relatively high in our models with low eddy viscosity (see Section 3). Analysis of the bottom panel of Fig. 20 clearly points that the 6467.5 K model display period-6 cycle behavior rather than period-3. This is further supported with the Fourier spectrum (Fig. 18). After pre-whitening with the fundamental mode and its harmonics (top panel of Fig. 18) a very strong signal is present at $1/3f_0$ and its harmonics. After pre-whitening we clearly detect signal at $1/6f_0$ (and harmonics), which is however, three order of magnitude weaker (middle panel of Fig. 18). After the next pre-whitening, signal is still present, which indicates that period-6 cycle is not strictly periodic, but displays irregular variation with very small amplitude. We note that only a fraction of Kelvin away chaotic band extends.

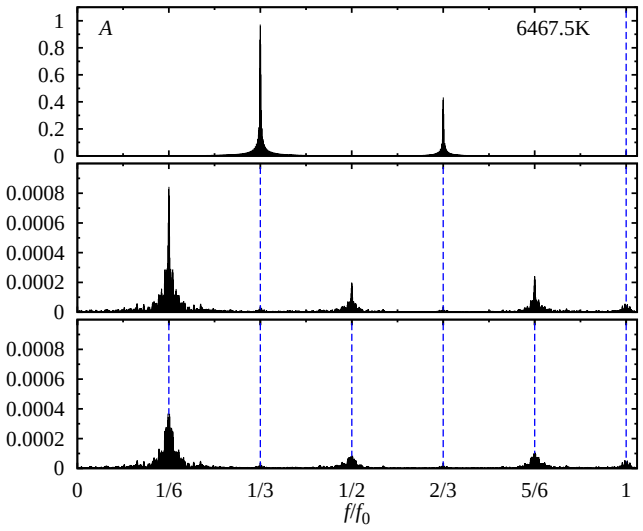

Figure 18. Fourier spectra for 6467.5 K model. Dashed lines show the location of pre-whitened frequencies (fundamental mode in the top panel).

The other model (6365.0 K) is not strictly periodic either, which is clear already from the bifurcation diagram and first return map (Fig. 11, brown points), which consists of nine separate and extended bands. Accordingly, strong signal at $1/9f_0$ (and harmonics) is present (top panel in Fig. 19). After pre-whitening, strong signal at $1/18f_0$ and its harmonics is present, which is not coherent however, as successive step of pre-whitening shows (bottom panel of Fig. 19). Fig. 21, showing the maximum radii over the 3 000 consecutive pulsation cycles, explains the origin of the $1/18f_0$ signal. The model switches intermittently between period-9 and period-18 cycle: starting from period-9 cycle

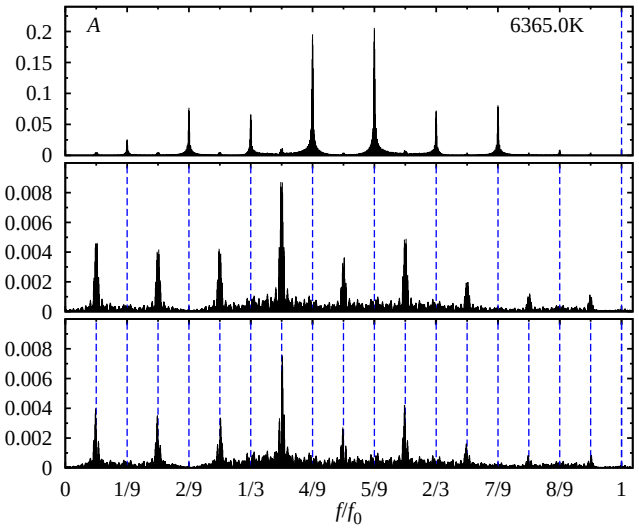

Figure 19. Fourier spectra for 6365.0 K model. Dashed lines show the location of pre-whitened frequencies (fundamental mode in the top panel).

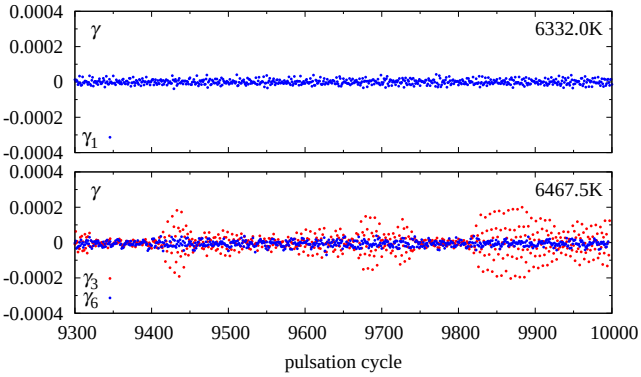

Figure 20. Bottom panel: kinetic energy growth rates, γ_k, summed over three (red points) or six (blue points) pulsation cycles, for 6467.5 K model. In the top panel kinetic energy growth rate for singly-periodic 6332.0 K model is plotted for comparison.

the subharmonic cycle grows up to some amplitude and then model switches back to cycle-9 behaviour. This is type-III intermittency (see Pomeau & Mannevile 1980, and Section 2), a result of collision between stable period-9 cycle and unstable period-doubled (period-18) cycle arising from subcritical period doubling bifurcation. Type-III intermittency is rarely observed in dynamical systems and in most cases concerns switching between period-1 cycle and period-2 cycle (e.g. Dubois, Rubio & Berge 1983). The very similar behaviour as in the case of 6365.0 K model was observed in electric circuits (see Thamilmaran & Lakshmanan 2002, their fig. 21).

5 LARGEST LYAPUNOV EXPONENTS

One of the key features of chaotic system is its sensitivity to initial conditions, which can be quantified using Lyapunov exponents. For the chaotic attractor, the two initially nearby trajectories diverge at an exponential rate given by the largest Lyapunov exponent, λ_1. To determine λ_1 for

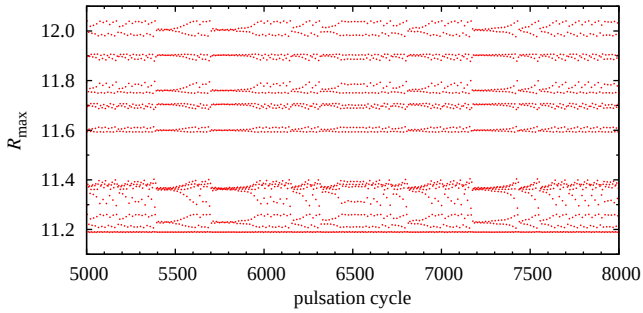

Figure 21. Values of maximum radii plotted over 3 000 pulsation cycles for 6365.0 K model showing type-III intermittency.

our models we used the code and algorithm developed by Rosenstein, Collins & De Luca (1993) based on the original algorithm of Grassberger & Procaccia (1983). Below we briefly describe the underlying idea and refer the reader to original papers for details.

We first reconstruct the attractor dynamics using the method of delays. We use the radius values equally spaced in time, R_i, to construct delay vectors, $\boldsymbol{x}_n$, in the embedding space:

$$\boldsymbol{x}_n = \left[R_{n-(m-1)J}, R_{n-(m-2)J}, \ldots, R_n\right].$$

m is the embedding dimension and J is time delay (or lag). The algorithm finds the close neighbours in the phase space, two points $\boldsymbol{x}_n$ and $\boldsymbol{x}_{n'}$ with sufficiently small distance between, $d_0 = \boldsymbol{x}_n - \boldsymbol{x}_{n'}$. For chaotic system the distance should grow exponentially in time, so that $d_{0+l} = \boldsymbol{x}_{n+l} - \boldsymbol{x}_{n'+l} \approx d_0 \exp(\lambda l)$, λ corresponding to the largest Lyapunov exponent. Analysis of results for many pairs of close neighbours leads to a robust estimate of λ_1.

For each model we have analysed only a section of the computed time series, of length T, expressed below as a multiple of the fundamental mode pulsation period. The default length of the analysed data is $\approx 1\,000$ pulsation cycles. The embedding dimension cannot be smaller than the physical dimension of the attractor. Provided m is high enough, its exact value should not affect the determined values of Lyapunov exponents. We find no systematic differences in the largest Lyapunov exponents computed assuming $m = 4$ and $m = 5$, and pick the latter value as the default (see also next paragraph). For the time delay we follow Rosenstein, Collins & De Luca (1993) and use J for which autocorrelation function drops to $1 - 1/e$ of its initial value.

Before running computations for all models we checked the sensitivity of λ_1 to chosen values of T, m and J, for one chaotic model of 6410.0 K. For the chosen dense time sampling ($\delta t = 0.01$d, more than 160 points per pulsation cycle) the lag resulting from autocorrelation function is $J = 27$. In the top row of Tab. 1 we show λ_1 computed assuming default values of T, m and J. Next, we have varied the values of these parameters and report the resulting largest Lyapunov exponents in the following rows of Tab. 1. We find that determination of λ_1 is robust and does not depend on exact values of the discussed parameters, provided that embedding dimension and lag are sufficiently high. Also, the chosen default length of the analysed time-series is sufficient, which we further verified computing λ_1 for all chaotic

Table 1. The largest Lyapunov exponents for the 6410.0 K model computed with different values of time-series length, T, embedding dimension, m, and lag, J.

T	m	J	λ_1 [d^{-1}]
1 000	5	27	0.217
670	5	27	0.212
1 400			0.208
1 000	2	27	0.136
	3		0.201
	4		0.212
	7		0.221
1 000	5	7	0.184
		17	0.210
		37	0.220
		47	0.220

models, assuming the default values for m and J, and two different lengths of time-series, the default one, of 1 000 pulsation cycles, and the shorter, of 670 pulsation cycles. The results are plotted in the bottom part of the bifurcation diagram displayed in Fig. 8, with thick black and thin blue lines respectively. Only for a few models a noticeable difference is present. We conclude that with $\sim 700 - 1\,000$ pulsation cycles the attractor dynamics is well probed.

The positive values of the largest Lyapunov exponents clearly establish the chaotic nature of our models. The typical values of λ_1 (Fig. 8) vary between $0.15\,\mathrm{d}^{-1}$ and $0.20\,\mathrm{d}^{-1}$. The largest values are slightly above $0.2\,\mathrm{d}^{-1}$ and are calculated for models between 6400.0 K and 6420.0 K. Within chaotic bands variation of λ_1 with effective temperature is not smooth. Large drops of λ_1 towards zero are seen, as expected, at the edges of periodic windows (for strictly periodic model $\lambda_1 = 0$). Smaller drops within chaotic domain may indicate a nearby periodic window, which was not detected because of too coarse resolution in effective temperature.

It is interesting to compare the computed values of λ_1 to those determined for two RV Tau stars and one Mira-type variable. Results obtained for these stars are collected in Tab. 2 together with λ_1 determination for one radiative chaotic model of Kovács & Buchler (1988). Ranges of λ_1 rather than single values are given as determination of λ_1 from real stellar data is much more sensitive to the values of embedding dimension, lag, etc. The reader is referred to tables in original papers (references are given below Table) for details.

The values of largest Lyapunov exponent determined for our models are typically two orders of magnitude larger than values determined for stars or a radiative model listed in Tab. 2. On the other hand, the pulsation periods of our models (always between $1.5 - 1.7$ d) are order or two orders of magnitude shorter (see third column in Tab. 2). In the context of pulsating stars however, it is more appropriate to use the length of a single pulsation cycle (pulsation period) as a unit of time. When expressed in units of inverse pulsation cycles rather than d^{-1}, the values of largest Lyapunov exponents of our models are comparable to the values determined for RV Tau/Mira-type stars. They are larger than for RV Tau type stars, but a factor ~ 4 smaller than for Mira type star.

Table 2. Literature determinations of the largest Lyapunov exponents for RV Tau/Mira-type stars and radiative model. Pulsation period is given in the third column (for RV Tau stars undoubled period is given).

star/type	λ_1 [10^{-4} d^{-1}]	period [d]	Ref.
R Cyg / Mira-type	$17 - 31$	≈430	1
R Sct / RV Tau	$14 - 22$	≈70	2
AC Her / RV Tau	$13 - 75$	≈37.5	3
D5200 / model	$34 - 55$	11.5	4

References: (1) Kiss & Szatmáry (2003) (tab. 2), (2) Buchler, Kolláth & Serre (1996) (tab. 1), (3) Kolláth et al. (1998) (tab. 1), (4) Serre, Kolláth & Buchler (1996) (tab. 1).

6 DISCUSSION

The non-linear stellar pulsation equations we solve, form a much more complex system than classical chaotic systems discussed in the literature. Yet the resulting dynamical scenario is qualitatively similar to that arising from the iteration of the simplest logistic map (compare the bifurcation diagrams in Figs. 1 and 8 and animations attached with the online version of this paper as supporting information). Most of conclusions about the origin of dynamical phenomena found in our models are drawn based on the analogies between our models and simpler systems for which strict analytical reasoning is possible. However, for some of the phenomena we detect, we do not find a satisfactory analogy. The appearance of period-6 window, extending between 6459.0 K and 6468.0 K, is one of them.

The scenario that is expected and that is encountered in many other systems, and is also present in the period-3 window (between 6421.0 K and 6438.0 K) is the following. First, a stable period-3 cycle is born together with unstable period-3 cycle. The stable branch undergoes a series of period doubling bifurcations to form three chaotic bands, which finally collide with the unstable period-3 cycle to form one chaotic band (Section 4.5). To the contrary, in the window at ≈ 6468.0 K, a stable period-6 cycle, which looks like two stable period-3 cycles born very close to each other, emerges from the chaos. We are not aware of any bifurcation that may lead to such scenario and of any other system showing such behaviour.

One of the possibilities is that in fact a pair of stable and unstable period-3 cycles is born, as expected, and stable cycle immediately undergoes a period doubling bifurcation. To check this, we have computed additional models in the interesting temperature range (with 0.1 K-step in effective temperature), but they display either chaos or a period-6 behaviour (in Section 4.6 we analysed one of these models). If the proposed scenario indeed takes place it must occur in a temperature range narrower than 0.1 K.

The situation at ≈ 6468.0 K looks even more complex. It seems that at this temperature we deal with discontinuity – the bifurcation diagram (Fig. 8) divides into two parts apparently decoupled from each other. On the cool side we clearly see a gradual evolution of the chaotic bands, divided, from time to time, by periodic windows. This gradual evolution seems to continue till 6468.0 K, but not for the band extending at higher effective temperatures. This behaviour may result from the coexistence of two attractors in the system. Note that by default we initialized all the models

along a sequence in the same manner (Section 3). It is possible that such initialization leads to different attractors for models cooler/hotter than 6468.0 K. To check the possible existence of other stable attractor(s) (with different basins of attraction), we have repeated the computation for many models, but with several different initializations. In all cases however, we finally arrived at the same attractor as in the case of our default initialization. At the moment the cause and nature of bifurcation we observe at 6468.0 K remains unclear.

The other phenomenon we have not discussed yet, is the appearance of chaos itself. The chaotic bands appear through a well understood period doubling route; the question is about the trigger. In the case of radiative models of Buchler & Kovács (1987) and Kovács & Buchler (1988), analysis of the Floquet coefficients clearly shows that the first period doubling bifurcation is caused by the half-integer resonance between pulsation modes (5 : 2 between fundamental and second overtone modes; Moskalik & Buchler 1990). The following cascade en route to chaos was not analysed. Moskalik & Buchler (1990) analysed a toy model of parametrically driven oscillator and showed that the first period doubling in such system results from the resonance and the following cascade is a result of increasing non-linearity. We note that the non-linearity may be the only cause of period doublings in classic chaotic systems void of internal resonances.

We do not have appropriate tools (Floquet coefficients) to proof that half-integer resonance is responsible for the period doubling of single-periodic pulsation we observe at the cool and the hot sides of our computation domain. The closest resonances are (Fig. 6) $\omega_8/\omega_0 = 9:2$ on the hot side of the computation domain and, $\omega_3/\omega_0 = 5:2$ and $\omega_5/\omega_0 = 7:2$ on the cool side. The loci of the $\omega_1/\omega_0 = 3:2$ resonance, causing the period doubled pulsation detected in a single BL Her star (Smolec et al. 2012) is located more than 300 K-off the hot side of the computation domain considered here and likely plays no role. We cannot exclude the possibility that non-linearity is the only cause of the observed behaviours.

The appearance of periodic windows is also very interesting and important for stellar pulsation studies. As in the case of period-doubled pulsation, resonances were also invoked as a possible explanation. In a recent study Plachy, Kolláth & Molnár (2013) proposed that a 27 : 20 resonance between the fundamental mode and the first overtone is responsible for a period-20 cycle behaviour they found in one of their RR Lyrae models (their model H; for other model they propose a 14 : 19 resonance). In this case however, a caution is needed, as inferences about the role of resonance are not based on firm theoretical grounds. The presence of first overtone cannot be deduced from the frequency spectrum. The role of resonance is most likely[2] deduced based on approximate coincidence of the model's location in the H-R diagram with the loci of the 27 : 20 resonance determined with linear pulsation periods. Since pulsation periods change in the non-linear regime, and fine-tuning of such high-order resonance is difficult, claims on the possible role of resonances must be supported with other (dynamical) arguments. We are not aware of any studies showing that such high-order resonances may indeed have a noticeable effect on stellar pulsations.

In a simpler explanation, period-k behaviour detected in the models, is an intrinsic property of non-linear, chaotic system. The ± 1 K neighbours of the discussed model of Plachy, Kolláth & Molnár (2013) show chaos and thus situation corresponds to periodic window within chaotic band, just as we report in this paper (Section 4.4), and as is found in many chaotic systems void of resonances. In chaotic systems the spectrum of periodic windows is dense (it is one of the key properties of chaotic systems; e.g. Petigen, Jürgens & Saupe 2004), but most of the windows are extremely narrow. Based on extreme similarity of our bifurcation diagram (Fig. 8), to bifurcation diagrams for other systems, we conclude that also in the case of our computations the spectrum of periodic windows is most likely dense, but most of the windows are extremely narrow (in effective temperature). With the default 1 K resolution of our model computation only few of the windows were detected (and most of them are narrower than 2 K). Studying linear periods we find no tight connection between location of the periodic windows and the loci of high-order resonances between low order pulsation modes. We conclude that existence of periodic windows is an intrinsic property of non-linear system studied in this paper. There is no need to invoke resonances to explain them.

7 OBSERVABILITY OF THE CHAOTIC PHENOMENA

Phenomena discussed in this paper are certainly exotic in the context of BL Her stars. Except of period doubling phenomenon detected in one star (Soszyński et al. 2011; Smolec et al. 2012), BL Her stars are single-periodic pulsators. We recall however, that existence of period-doubled BL Her star was predicted 20 years before its discovery (Buchler & Moskalik 1992). The future detection of other, more complex dynamical phenomena in these stars cannot be excluded.

Period doubling and irregular brightness variations are common in higher luminosity siblings of BL Her stars, namely in more luminous type II Cepheids of RV Tau type and in semi-regular variables. Period doubling is a characteristic feature of RV Tau stars which, in addition, show irregular variation. Chaos was reported in several stars of these types (Buchler, Kolláth & Serre 1996; Kolláth et al. 1998; Buchler, Kolláth & Cadmus 2004; Kiss & Szatmáry 2003). Our models suggest that other phenomena, intrinsic to chaotic dynamics, may also occur in these groups of stars. Particularly interesting would be the discovery of period-k behaviour (with k other than 2) and of intermittency.

Period-k behaviour may arise either within a period doubling cascade or within chaotic band. A possible period-4 behaviour in RV Tau type star, supporting the period-doubling transition to chaos scenario, was reported by Pollard et al. (2000). Unfortunately, our unpublished analysis of the OGLE-III data for this star does not confirm the detection. Models indicate that in the case of period doubling cascade the domains of period-k behaviour get nar-

[2] Plachy, Kolláth & Molnár (2013) do not discuss in detail how the connection between the periodic pulsation and resonances is made.

rower as k increases, making the detection less probable for larger k. Also most of the periodic windows within chaotic domain are very narrow. Nevertheless, in our opinion, the firm detection of period-4 behaviour in RV Tau stars is only a matter of time.

From observers point of view, the strongest evidence for period-k behaviour would be the presence of additional signal in the frequency spectrum, at f_0/k and its harmonics. The difficulty arises for long-period variables, as very long time-series is necessary to get sufficient resolution in the sub-harmonic part of the frequency spectrum (i.e. in a range $[0,\ f_0]$). In addition, the effect may be obscured by irregular variability on top of period-k behaviour, as is commonly observed in RV Tau stars (see eg. lightcurves in Soszyński et al. 2011). In these stars, a sporadic switching of the deep and shallow minima also occurs (Wallerstein 2002) which is yet another difficulty in the analysis. Therefore, inspection of the time-series, folding the light curve with multiple of the basic period, are invaluable tools to search for the effect. This however requires not only long time-series, but also well sampled time-series. In this respect the projects aimed at long-term and regular monitoring of the sky or individual stars, such as OGLE (Udalski et al. 2008), EROS (e.g. Beaulieu et al. 1995), ASAS (Pojmanski 2002), or programs led by amateur associations of variable star observers (e.g. AAVSO) are extremely important and should be continued as long as possible. It is worth noting that the observations of the only stars rigorously analysed for the presence of chaotic dynamic (i.e. those from Tab. 2) were all collected by amateur astronomers and in all cases covered more than 10 years (up to a century for R Cyg).

Based on our rather restricted model survey we cannot predict the expected amplitude of brightness alternations within period-k cycle. In period-doubled RV Tau stars the amplitude of alternations vary from a hundredth of magnitude to few tenths of magnitude. More precise the photometry, larger the chance to detect the smaller effect.

Long-lasting and frequent observations of the stars are also crucial for the possible detection of intermittency. Models indicate that the intervals of apparently periodic/chaotic behaviour may last many tenths of pulsation cycles which, as pulsation periods of the luminous stars are long, requires a very long monitoring. Again, intermittency is expected in the narrow domains close to the edges of periodic windows and thus probability of its detection is certainly very small.

8 SUMMARY

The BL Her models discussed in this paper fall along a single stripe of constant luminosity in the H-R diagram and cover a range of only $\approx$150 K. Yet they display a wealth of dynamical behaviours characteristic for deterministic chaos. Many of the discussed phenomena are detected for the first time in the context of stellar pulsation models. It was possible because our model survey was dedicated to study such phenomena – a tiny step in effective temperature, sometimes as small as 0.1 K (and 1 K max), allowed to follow the dynamical evolution of the system from single-periodic pulsation, through period doubling cascade to well developed chaotic regime, and back to single-periodic pulsation. The chaotic regime turned out to be a gold-mine of interesting dynamical phenomena. We found several periodic windows (with cycle-3, 5, 6, 7 and 9 behaviours). We stress that the existence of periodic windows is not related to resonances among pulsation modes, but is an intrinsic property of a chaotic system. At the edges of the largest period-3 and period-6 windows we have found intermittent behaviour and crises bifurcations. Particularly interesting is intermittency – a sporadic switching between two qualitatively different behaviours. In type-I intermittency intervals of apparently periodic (period-k, in general) behaviour are interrupted with bursts of chaos. In type-III intermittency the oscillations switch between two periodic cycles. In our models we detected switching between period-9 and period-18 cycles.

Detection of the discussed phenomena in the stars would be extremely interesting, however it requires a long and regularly sampled time series. The already available data from projects such as OGLE offer the best opportunity for a successful search.

ACKNOWLEDGMENTS

Model computations presented in this paper were conducted on the psk computer cluster in the Copernicus Centre, Warsaw, Poland. This research is supported by the Polish Ministry of Science and Higher Education through Iuventus+ grant (IP2012 036572) awarded to RS. PM is supported by the Polish National Science Centre through grant DEC-2012/05/B/ST9/03932.

REFERENCES

Beaulieu J.P., et al., 1995, A&A, 303, 137
Becker J., Rödelsperger F., Weyrauch Th., Benner H., Just W., Cenys A., 1999, Phys. Rev. E, 59, 1622
Bier M., Bountis T.C., Phys. Lett. A, 104, 239
Buchler J.R., Kovács G., 1987, ApJL, 320, L57
Buchler J.R., Moskalik P., 1992, ApJ, 391, 736
Buchler J.R., Kolláth Z., 2011, ApJ Lett., 731, 24
Buchler J.R., Kolláth Z., Serre T., 1996, ApJ, 462, 489
Buchler J.R., Kolláth Z., Cadmus R.R., 2004, ApJ, 613, 532
Collet P., Eckmann J.-P., Lanfold III O.E., 1980, Comm. Math. Phys., 76, 211
Collet P., Eckmann J.-P., Koch H., 1981, J. Stat. Phys., 25, 1
Dubois M., Rubio M.A., Berge P., 1983, Phys. Rev. Lett., 51, 1446
Eckmann J.-P., 1981, Rev. Modern Phys., 53, 643
Feigenbaum M.J. 1983, Physica D, 7, 16
Grassberger P., Procaccia I. 1983, Physica D, 9, 189
Grebogi C., Ott E., Yorke J.A. 1982, Phys. Rev. Lett., 48, 1507
Hilborn R.C., 2000, "Chaos and Nonlinear Dynamics. An Introduction for Scientists and Engineers", second Edition, Oxford University Press
Kiss L.L., Szatmáry K., 2003, A&A, 390, 585
Kolláth Z., Buchler J.R., Serre T., Mattei J., 1998, A&A, 329, 147
Kovács G., Buchler J.R., 1988, ApJ, 334, 971
Kuhfuß R., 1986, A&A, 160, 116

Lenz P., Breger M., 2005, Comm. in Asteroseismology, 146, 53
Letellier C., Gouesbet G., Soufi F., Buchler J.R., Kolláth Z., 1996, Chaos, 6, 466
Lorenz E.N, 1963, J. of the Atm. Sci., 20, 130
Mannevile P., Pomeau Y., 1979, Phys. Lett. A, 75, 1
May R.M., 1976, Nature, 261, 459
Moskalik P., Bucher J.R., 1990, ApJ, 355, 590
Plachy E., Kolláth Z., Molnár L., 2013, MNRAS, 433, 3590
Pojmanski, G. 2002, Acta Astron., 52, 397
Pollard K.R., et al., 2000, ASP Conf. Ser., 203, 89
Pomeau Y., Mannevile P., 1980, Comm. Math. Phys., 74, 189
Petigen H.-O., Jürgens H., Saupe D, 2004, "Chaos and Fractals", secon edition, Springer-Verlag, New York
Rosenstein M.T., Collins J.J., DeLuca C.J. 1993, Physica D, 65, 117
Serre T., Kolláth Z., Buchler J.R., 1996, A&A, 311, 845
Seydel R., 2010, "Practical Bifurcation and Stability Analysis", third edition, Springer, New York
Smolec R., Moskalik P., 2008, Acta Astron., 58, 193
Smolec R., Moskalik P., 2012, MNRAS, 426, 108
Smolec R., Moskalik P., 2014, IAU Symp. No 301, p. 489
Smolec R., et al., 2012, MNRAS, 419, 2407
Soszyński I., et al., 2011, Acta Astron., 61, 285
Thamilmaran K., Lakshmanan M., 2002, Int. J. of Bifurcation and Chaos, 12, 783
Udalski A., Szymanski M., Soszynski I., Poleski R., 2008, Acta Astron., 58, 69
Wallerstein G., 2002, PASP, 114, 689

SUPPORTING INFORMATION

Additional Supporting Information may be found in the online version of this article:

Animation 1: The animation shows the evolution of first return map for logistic equation as control parameter k is increased from 2.8 to 4. Note that smaller step is used within chaotic regime.

Animation 2: The animation shows the evolution of first return map for BL Her models discussed in the paper. Note the different, smaller effective temperature step at the edges of period-3 window.